1 Magnetoelectric materials for miniature, wireless neural stimulation at
2 therapeutic frequencies
3

4   Amanda Wickens[1,2], Benjamin Avants[2], Nishant Verma[3], Eric Lewis[2], Joshua C. Chen[3],
5   Ariel K. Feldman[4,5], Shayok Dutta[2], Joshua Chu[2], John O'Malley[6], Michael Beierlein[6],
6   Caleb Kemere[2,3], Jacob T. Robinson[1,2,3,7]
7

8   [1]Applied Physics Program, Rice University, Houston, Texas, USA, [2]Department of Electrical and
9   Computer Engineering, Rice University, Houston, Texas, USA, [3]Department of Bioengineering, Rice
10 University, Houston, Texas, USA, [4]Department of Computer Science, Rice University, Houston, Texas,
11 USA, [5]Department of Cognitive Science, Rice University, Houston, Texas, USA, [6]Department of
12 Neurobiology and Anatomy, McGovern Medical School at UTHealth, Houston, Texas, USA,
13 [7]Department of Neuroscience, Baylor College of Medicine, Houston, Texas, USA
14

15 **A fundamental challenge for bioelectronics is to deliver power to miniature**
16 **devices inside the body. Wires are common failure points and limit device**
17 **placement. Wireless power by electromagnetic or ultrasound waves must**
18 **overcome absorption by the body and impedance mismatches between air,**
19 **bone, and tissue. Magnetic fields, on the other hand, suffer little absorption by**
20 **the body or differences in impedance at interfaces between air, bone, and**
21 **tissue. These advantages have led to magnetically-powered stimulators based**
22 **on induction or magnetothermal effects. However, fundamental limitations in**
23 **these power transfer technologies have prevented miniature magnetically-**
24 **powered stimulators from applications in many therapies and disease models**
25 **because they do not operate in clinical "high-frequency" ranges above 20 Hz.**
26 **Here we show that magnetoelectric materials – applied for the first time in**
27 **bioelectronics devices – enable miniature magnetically-powered neural**
28 **stimulators that operate at clinically relevant high-frequencies. As an**
29 **example, we show that ME neural stimulators can effectively treat the**
30 **symptoms of a Parkinson's disease model in a freely behaving rodent. We also**
31 **show that ME-powered devices can be miniaturized to sizes smaller than a**
32 **grain of rice while maintaining effective stimulation voltages. These results**
33 **suggest that ME materials are an excellent candidate for wireless power**
34 **delivery that will enable miniature neural stimulators in both clinical and**
35 **research applications.**
36

37 Wireless neural stimulators have the potential to provide less invasive, longer
38 lasting interfaces to brain regions and peripheral nerves compared to battery-
39 powered devices or wired stimulators. Indeed, wires are a common failure point for
40 bioelectronic devices. Percutaneous wires present a pathway for infection[1] and
41 implanted wires can also limit the ability of the stimulators to move with the tissue,
42 leading to a foreign body response or loss of contact with the target tissue[2,3].
43 Additionally, chronic stress and strain on wires, particularly for devices in the
44 periphery, can lead to failure in the wire itself or its connection to the stimulator[4]. In
45 small animals like rats and mice, wires used to power neural stimulators can
46 interfere with natural behavior, particularly when studying social interaction
47 between multiple animals[5].

48
49 One of the primary challenges for wireless neural stimulators is to create efficient
50 miniature devices (< 1 cm in length) that operate reliably beneath bone and tissue
51 as an animal or human patient engages in normal activity. At lengths of less than 1
52 cm, devices could be fully implanted in the periphery and be light enough to allow
53 for unrestricted animal behavior; however for devices this small, power delivery
54 remains a challenge. Efficient power transfer with propagating electromagnetic
55 waves requires antennas with feature sizes comparable to the electromagnetic
56 wavelength. Thus, for sub-millimeter devices, such as the proposed RF powered
57 "neurograins[6]," effective power-transfer frequencies lie in the GHz range, where
58 electromagnetic radiation is absorbed by the body[7]. Absorption of this radio-
59 frequency electromagnetic energy limits the amount of power that can be safely
60 delivered to implants deep inside tissue[7]. As a result, researchers typically turn to
61 magnetic induction or batteries to power implanted devices; however, these
62 techniques also limit the degree of miniaturization. Batteries increase the size of the
63 device and add considerable weight. Additionally, batteries require replacement or
64 charging, which can limit the potential uses. Inductively coupled coils, on the other
65 hand, can be made smaller and lighter than batteries, however; the power a
66 receiving coil can generate is directly related to the amount of flux captured by the
67 area of the coils. Thus, when the receiver coils are miniaturized, the output power
68 reduces and becomes more sensitive to perturbations in the distance or angle
69 between the transmitter and receiver[8]. For example, Freeman et al. demonstrated
70 that small inductive coils less than 1 mm in diameter can power stimulators for the
71 sciatic nerve in anesthetized rats[9]; however, in its present form, this device would
72 have difficulty providing stable stimulation in freely moving animals due to the
73 reduced power coupling efficiency that accompanies changes in the angle and
74 distance between the receiver and transmitter coils.
75
76 Additionally, for neural stimulators to treat a number of neurological disorders like
77 Parkinson's Disease (PD), obsessive-compulsive disorder, and epilepsy, they must
78 operate safely and effectively in the high-frequency "therapeutic band" between 100
79 and 200 Hz[10-12]. This type of high-frequency neural stimulation is challenging
80 because charge on the electrode must be dissipated between successive stimulation
81 pulses to prevent electrolysis, tissue damage, and changes to the local pH[13]. Charge
82 dissipation at high-frequencies is accomplished by using a biphasic stimulus
83 waveform that actively or passively charges and discharges the electrode with each
84 cycle. Indeed all clinically approved electrical neural stimulation therapies in this
85 therapeutic band use various forms of "charge balanced" biphasic stimulation
86 waveforms[14].
87
88 Recently, several promising alternatives to magnetic induction and batteries have
89 enabled miniature neural stimulators; however, these approaches have yet to
90 demonstrate *in vivo* operation in the therapeutic high-frequency band in freely
91 moving animals. Montgomery et al. and Ho et al. have shown that one can use the
92 mouse body as an electromagnetic resonant cavity to effectively transfer energy to
93 sub-wavelength scale devices implanted inside the animal[15,16]. This approach is

94   particularly effective to drive tiny LEDs for optogenetic stimulation. However,
95   because the electrical waveform is monophasic, electrical stimulation has been
96   limited to < 20 Hz. Using superparamagnetic nanoparticles to absorb energy from
97   high-frequency (500 kHz) magnetic fields[17], one can heat specific regions of the
98   brain [18,19] in freely moving animals[19]. This local heat can stimulate neural activity
99   when the targeted brain region is genetically modified to respond to changes in
100 temperature[18,19]. However this approach requires transgenesis, which adds
101 regulatory complexity and has yet to show high-frequency operation due the
102 requirement for the tissue to cool between stimulation intervals. Ultrasound
103 provides a promising and efficient method to power bioelectronic implants because
104 ultrasound wavelengths are 10^5 times smaller than electromagnetic waves at the
105 same frequency allowing sub-millimeter-sized devices to have wavelength-scale
106 piezoelectric antennas [20,21]. However, implementation of these "neural dust" motes
107 can be challenging in freely moving animals because the impedance mismatch
108 between air, bone, and tissue requires contact between soft tissue and the
109 ultrasound transducer for efficient power transfer. As a result, there has yet to be a
110 demonstration of ultrasound-powered neural stimulators in freely moving
111 animals[22].
112
113 Here we show that magnetoelectric (ME) materials enable the first magnetically
114 powered miniature neural stimulators that operate in the therapeutic high-
115 frequency band. Similar to inductive coils, these materials transform a magnetic
116 field to an electric field, but instead of using an implanted coil we use a material that
117 generates a voltage via mechanical coupling between magnetostrictive and
118 piezoelectric layers in a thin film. Namely, the magnetic field generates strain in the
119 magnetostrictive layer as the magnetic dipoles align with the applied field. That
120 strain exerts a force on the piezoelectric layer, which generates a voltage (Fig. 1). By
121 exploiting this transduction mechanism, magnetoelectrics do not suffer from the
122 same miniaturization constraints as coils and can be driven by weak magnetic fields
123 on the order of a few millitesla. These properties have led researchers to propose
124 magnetoelectrics as a promising material for bioelectronic implants[23–27]. Here we
125 demonstrate the first proof-of-principle wireless neural stimulators based on ME
126 materials in a freely behaving rodent model for Parkinson's Disease (PD), and that
127 these materials could power miniature devices deep within the human brain.
128
129 **Fabrication and characterization of ME stimulators**
130
131 We fabricated proof-of-principle ME stimulators by bonding a rectangular
132 magnetostrictive layer (Metglas) to a platinum coated piezoelectric layer,
133 polyvinlydine fluoride (PVDF). We then encapsulated the films in a protective
134 parylene-C layer (8-10 µm thick) (Fig. 1a, see Methods). We used PVDF layers
135 between 28 and 110 µm, which yielded total device thicknesses between 50-150
136 µm. When we measured the voltage across the film, we found a dramatic voltage
137 increase when the applied magnetic field frequency, matches an acoustic resonant
138 frequency (Fig. 1b). Because the resonant frequency is proportional to the inverse of
139 the film length, we can design multiple films and selectively activate them by

140 changing the stimulus frequency (Fig. S2b). Using this principle, we can use different
141 magnetic field frequencies to activate separate devices that may be in different areas
142 of the body, or create biphasic stimulators by interleaved resonant stimulation of
143 two different films, with each film driving either the positive or negative phase of
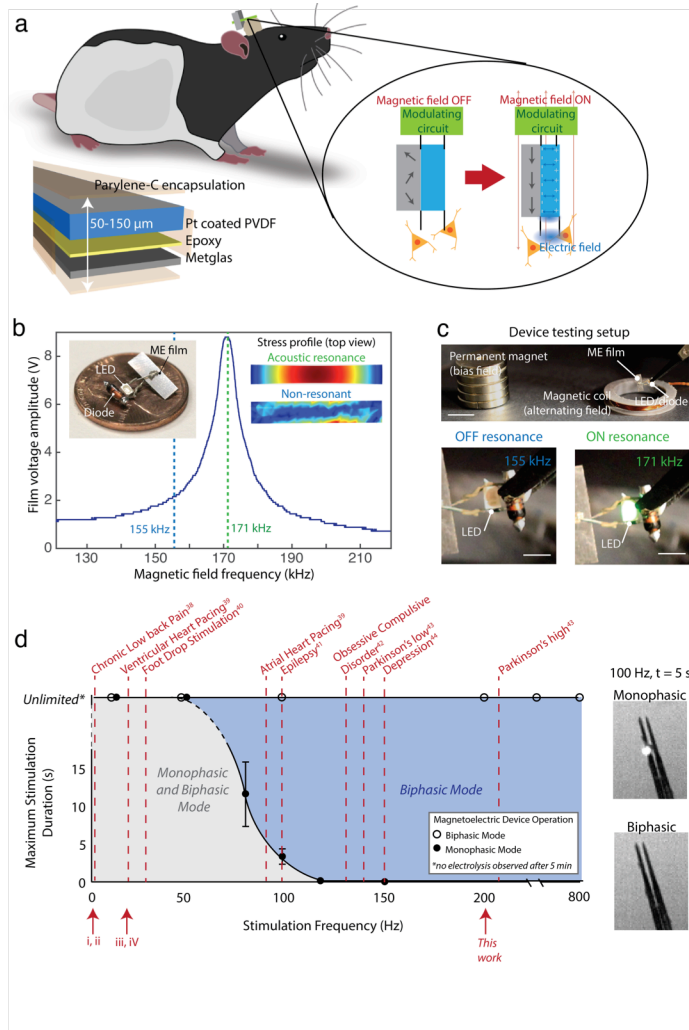144 the neural stimulus.

Figure 1 | ME films convert alternating magnetic fields into a voltage. (a) Diagram of a ME device on a freely moving rat for wireless neural stimulation. The active ME element consists of piezoelectric PVDF (blue) and Metglas (gray) laminate encapsulated by Parylene-C. Inset shows the operating principle whereby the strain produced when magnetizing the gray magnetostrictive layer is transferred to the blue piezoelectric layer, which creates a voltage across the film. (b) Example of a resonant response curve for a ME film showing that the maximum voltage is produced when the magnetic field frequency matches an acoustic resonance at 171 kHz. Photograph inset shows an example of an assembled ME stimulator. The "Stress profile" inset shows a top view of the stress produced in a ME film as calculated by a finite element simulation on and off resonance (COMSOL). (c) Device testing setup with a permanent magnet to apply a bias field and an electromagnetic coil to apply an alternating magnetic field (scale bars: upper = 1 cm, lower = 2 mm) (d) Maximum stimulation duration (using a 400 µs/phase pulse repeated at increasing frequencies) for a ME device in biphasic and monophasic operation. Maximum stimulation time is determined by time of electrolysis on a stereotrode in saline as evidenced by gas bubbles (error bars +/- 1 standard deviation for n=4 trials). Dashed lines indicate frequencies of electrical stimulation used in various clinical applications, showing that biphasic operation is necessary for many clinically relevant applications. Roman numerals indicate stimulation frequencies demonstrated by previously published miniature magnetic stimulators (i: Magnetothermal, Chen et. al, 2015, ii: Magnetothermal, Munshi et. al, 2017, iii: Mid-Field Optogenetics, Montgomery et. al, 2015, iv: RF Inductive Coupling, Freeman et. al, 2017).

145
146 We can further enhance the voltage generated by the ME films by applying a
147 constant bias field with a permanent magnet or an electromagnet (Fig. 1c). Because
148 the strain in the magnetostrictive material is a sigmoidal function of the magnetic
149 field strength, the change in voltage produced by the alternating field is largest
150 when the field oscillates about the midpoint of the sigmoid (Fig. S1)[28,29]. Thus, we
151 use a bias field to offset the magnetic field near the center of the sigmoidal
152 magnetostrictive response curve. This bias field allows us to generate therapeutic
153 voltage levels while applying a small (few mT) alternating magnetic field using an
154 electromagnetic coil and custom control circuitry that specifies the frequency and
155 timing of the alternating magnetic field (Fig. S3).
156
157 To identify the operational frequencies for our ME stimulators we tested them in
158 saline and found that with a biphasic stimulation waveform we could apply constant
159 stimulation up to at least 800 Hz without significant hydrolysis. For this test we
160 operated either one film for monophasic stimulation or two films for biphasic
161 stimulation attached to a stereotrode (Microprobes) in saline (see Methods). We
162 then measured the time at which we could see bubbles at the electrode tip resulting
163 from hydrolysis. This hydrolysis event indicates conditions that would lesion the
164 surrounding tissue. We found that with a monophasic stimulation waveform
165 stimulation frequencies above 50 Hz produced hydrolysis while biphasic charge-
166 balanced stimulation showed no hydrolysis up to the maximum tested frequency of
167 800 Hz. Compared to previously demonstrated miniature magnetic neural
168 stimulators, the biphasic ME devices shown here are the first to access the high-
169 frequency bands used for clinical applications like the treatment of Parkinson's
170 disease and obsessive-compulsive disorder (Fig 1d).
171
172 An additional challenge for any wirelessly powered neural stimulator is to maintain
173 a well-regulated stimulation voltage. This challenge is especially prevalent as
174 devices become small, which often reduces the power transfer efficiency resulting in
175 a greater sensitivity to the alignment between the device and power transmitter. ME
176 materials offer two main advantages that can enable stable and effective stimulation
177 even as devices become small and move with respect to the driver coils:
178
179 First, ME devices generate voltages well in excess of the effective stimulation
180 potential, allowing them to be effective even if the materials are misaligned with the
181 driver coils. At resonance, we have measured ME voltages in excess of 30 V at a field
182 strength of only 1 mT (Fig. S2c, d). Because effective stimulation voltages are usually
183 between 1-5 V, we can cap the applied voltage to this effective stimulation range
184 using an LED or Zener diode. As long as the voltage generated by the ME film is
185 greater than or equal to the capping voltage, we will apply approximately the same
186 stimulus voltage regardless of the angle or distance between the driver coil and the
187 ME film. For a typical film we found that we could reorient the film by +/- 80
188 degrees and maintain voltages in excess of 3 V (Fig. S1h). This large angular
189 tolerance is aided by the large magnetic permeability of the Metglas layer, which

190 helps to direct the magnetic field lines along the long axis of the film, where they are
191 most effective at creating a magnetostrictive response.
192
193 Second, the voltage generated by a piezoelectric material depends on the thickness
194 of the piezoelectric layer and not the area of the film[30], allowing us to fabricate small
195 magnetoelectric films that generate roughly the same stimulation voltage as larger
196 devices. Figure S2 shows the peak voltage generated and quality factor for ME films
197 of different areas. We found that, for a 52 μm thick PVDF layer, the voltage remains
198 around 10 V even as the film length decreases. Variations of +/- 40 % in peak
199 voltage and quality factors are likely due to defects produced during film
200 fabrication, which may be reduced with improved manufacturing. We also verified
201 that the output voltage depends only on the piezoelectric film thickness by
202 measuring the peak voltages from ME devices with three different thicknesses of
203 PVDF: 28 μm, 52 μm, and 110 μm. As expected, we see that the peak voltage
204 increases linearly with the PVDF thickness and is independent of the film length. We
205 calculated (and experimentally confirmed) that the power generated by a ME device
206 is proportional to the film width for a given thickness and a length-to-width ratio >3
207 (see Fig. S2f). Despite the decrease in power as films become smaller, we calculate
208 that films less than 1 cm long can generate up to 4 mW, which is more than
209 sufficient for many wireless applications including neural stimulation[31].
210
211 **Monophasic stimulation by ME films evoke action potentials *in vitro***
212
213 Using fluorescence microscopy to image voltage in cultured cells, we found that
214 monophasic stimulation for 50 ms at 100 Hz by ME films reliably stimulated action
215 potentials (APs). For these experiments we used "spiking" human embryonic kidney
216 (HEK) cell lines that were modified to express sodium and potassium channels.
217 These cells have spike-like electrical waveforms that are rectangular in shape and
218 can last for a few seconds depending on the confluency of the culture[32]. To
219 determine the relative timing between magnetic stimulation and action potential
220 generation, we transfected these cells with ArcLight[33]-a genetically encoded voltage
221 indicator that allows us to measure action potentials using fluorescence microscopy.
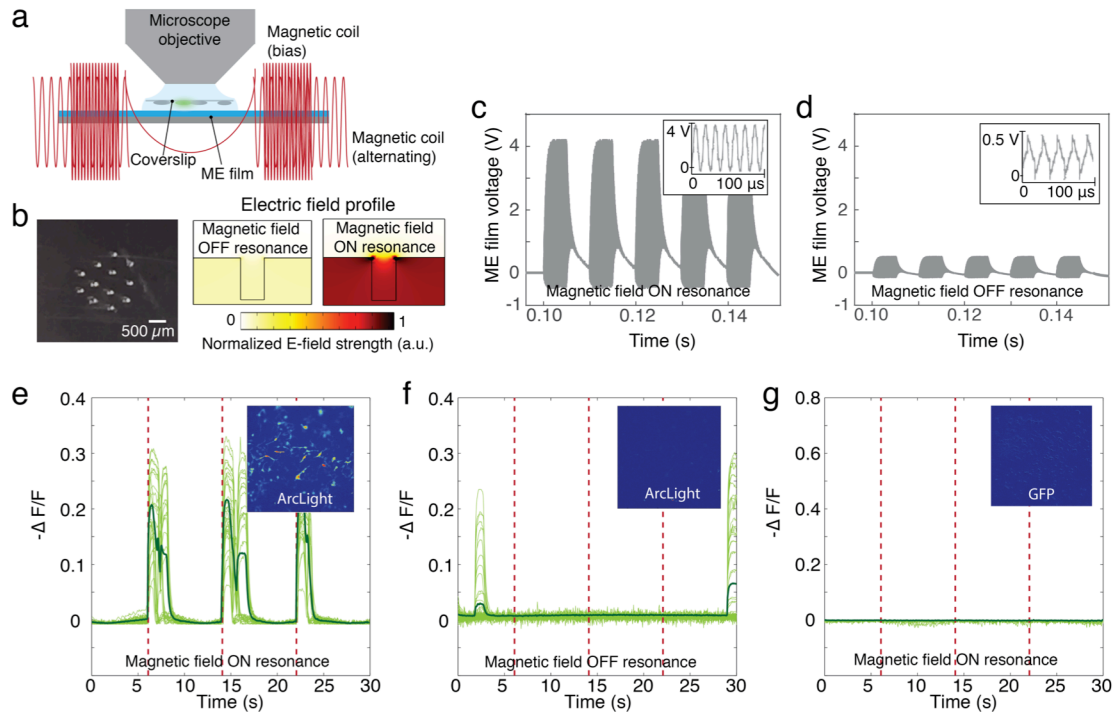222

Figure 2 | Monophasic ME stimulators activate cells in vitro (a) Schematic of the experimental setup (b) Microscope image of holes stamped into the ME film and finite element simulation of the electric field shows that the holes produce fringing electric fields that overlap the culture cells (c) Voltage across the ME film when the magnetic field is on resonance and (d) off resonance. Insets show a zoom in of the high frequency carrier waveform. (e-g) Fluorescence from spiking HEKs transfected with ArcLight show action potentials are triggered by the ME film driven at resonance (e), but not when the film is driven off resonance (f). Fluorescence from HEK cells transfected with GFP show no response when the ME film is driven on resonance confirming that the measured ArcLight response is the result of a change in transmembrane potential and not an artifact of the magnetic field or acoustic resonance of the ME film.

223   To image fluorescence while we applied magnetic fields, we developed an
224   experimental setup that allows us to place cells and ME films beneath an objective
225   lens at the center of a 10 cm long solenoid with a 3 cm gap in the center. This
226   configuration allowed us to place ME films, cells, and the objective lens at the center
227   of the applied magnetic field (Fig. 2a). Two slightly larger coils placed on either side
228   of the gap provide the constant bias field.
229
230   We then approximated an implanted ME stimulator using two experimental
231   configurations: 1) growing cells directly on the ME film (Fig. S4) and 2) laying a
232   coverslip with adherent cells on top of the ME film (Fig. 2). To culture cells directly
233   on the ME film, we coated the top parylene layer with poly-l-lysine. The healthy
234   proliferation of HEKs on the ME device indicates that this encapsulation approach
235   prevents the ME materials from limiting cell growth (Fig. S4b). However, in a typical
236   use case, the target cells may not adhere to the ME stimulator, so we also tested the
237   response of cells laid on top of the ME materials. In this configuration we first grew
238   the cells on coverslips for 3-5 days before inverting the coverslips and laying them
239   on the ME for testing (Fig. 2, see Methods).

240
241 To create fringing electric fields that interact with the cultured cells, we stamped
242 holes in the ME film (Fig. 2b). The films were otherwise fabricated as described
243 above (Fig. 1, Methods). In experiments using ME films and Pt electrodes we found
244 that high-frequency biphasic stimulation at the ME resonance frequency (typically
245 20-150 kHz) was not effective to stimulate APs in cultured HEKs, as predicted by the
246 low-pass filtering properties of the cell membrane[9]. To create an effective
247 monophasic stimulus waveform, we used a Schottky diode to rectify the voltage to
248 create entirely positive or negative voltage waveforms depending on the diode
249 direction. This rectified waveform has a slowly varying monophasic envelope in the
250 <500 Hz frequency band where cells are responsive (Fig. 2c,d).
251
252 For both cells grown directly on the ME films and those placed in contact we found
253 that five stimulation pulses with an envelope frequency of 100 Hz consistently
254 stimulated APs in the spiking HEK cells (Fig. 2e, S4c, Supplementary Video 1).
255 Critically, this 10-500 Hz stimulation frequency is spans the therapeutic window for
256 many deep brain stimulation treatments[34], and difficult to achieve with other
257 wireless stimulators that compensate for low-efficacy energy harvesting by charging
258 on-board capacitors[35]. For our experiments, the carrier frequency of the magnetic
259 field was at the resonant frequency of the device, which varied between 20-40 KHz
260 depending on device length. To test stimulation reliability, we repeated the 5-pulse
261 stimulus three times over a period of 30 seconds. We observed APs for each
262 stimulation pulse in n = 43 cells on coverslips and n = 144 cells grown on films. We
263 confirmed that the APs stimulated by the ME film were in fact the result of resonant
264 excitation of the film and not an artifact of the applied magnetic fields by imaging
265 voltage-sensitive fluorescence when the magnetic field was tuned off of the resonant
266 frequency. For non-resonant excitation we observed no correlation between the
267 applied field and fluorescently detected APs in the spiking HEKs (Fig. 2f, S4d),
268 supporting the conclusion that APs were stimulated by the ME film at resonance. We
269 also confirmed that the fluorescent signal recorded indeed represents the voltage-
270 dependent ArcLight response by imaging cells transfected with voltage-independent
271 cytoplasmic GFP. These cells showed no change in fluorescence when the films were
272 driven at the resonant frequency (Fig. 2g).
273
274 **Biphasic stimulation by ME films evoke action potentials in brain slices**
275
276 As described above, biphasic stimulation is preferred for most applications due to
277 the desire to create a charge-balanced stimulus that reduces charge buildup and
278 undesired electrochemical reactions at the electrode surface[13]. While the voltage
279 waveform produced by ME films at resonance is biphasic, these resonant
280 frequencies (typically 20 – 150 kHz) are too high to produce reliable cell
281 stimulation, as described above. To create an effective biphasic stimulus in the
282 therapeutic window (100 – 200 Hz), we use two films with distinct resonant
283 frequencies connected to the same stimulating electrodes (Fig. 3a). The first film is
284 attached to a full wave rectifier, which is oriented to generate a positive pulse, while
285 the second film is attached to a full wave rectifier that generates a negative pulse.

286   The transistors block currents generated by one film from propagating through the
287   circuitry attached to the other film, ensuring that only one half of the circuit is active
288   at a time. By switching the magnetic field frequency between the two ME resonance
289   frequencies, we can alternate positive and negative phase stimulation to create a
290   biphasic neural stimulator (Fig. 3b-d). In this case the residual charge of -2.3 nC,
291   which discharges in <2 ms, implies that this stimulator can safely operate at
292   frequencies up to >500 Hz without accumulating charge.
293
294   We found that our biphasic ME stimulator is capable of repeatable neural
295   stimulation using neocortical brain slices derived from mice that express the
296   genetically encoded calcium indicator GCaMP3 in GABAergic neurons. To image
297   neural activity following ME stimulation we inserted a stereotrode attached
298   biphasic ME stimulator described above while we imaged GCaMP activity using
299   fluorescence microscopy (Fig. 3e-g, Methods). We chose neural stimulation
300   parameters similar to those commonly used for deep brain stimulation[34]: 100
301   biphasic pulses at 200 Hz with each phase lasting 175µs. When the magnetic field
302   was on we observed a corresponding increase in fluorescence in n=23 recordings in
303   neocortical layer 5 consistent with activity-mediated calcium increases
304   (Supplementary Video 2). Following bath application of tetrodotoxin (TTX , 500
305   nM) fluorescence increases were completely blocked in n=9 recordings confirming
306   that ME stimulation reliably evoked sodium-channel dependent action potentials in
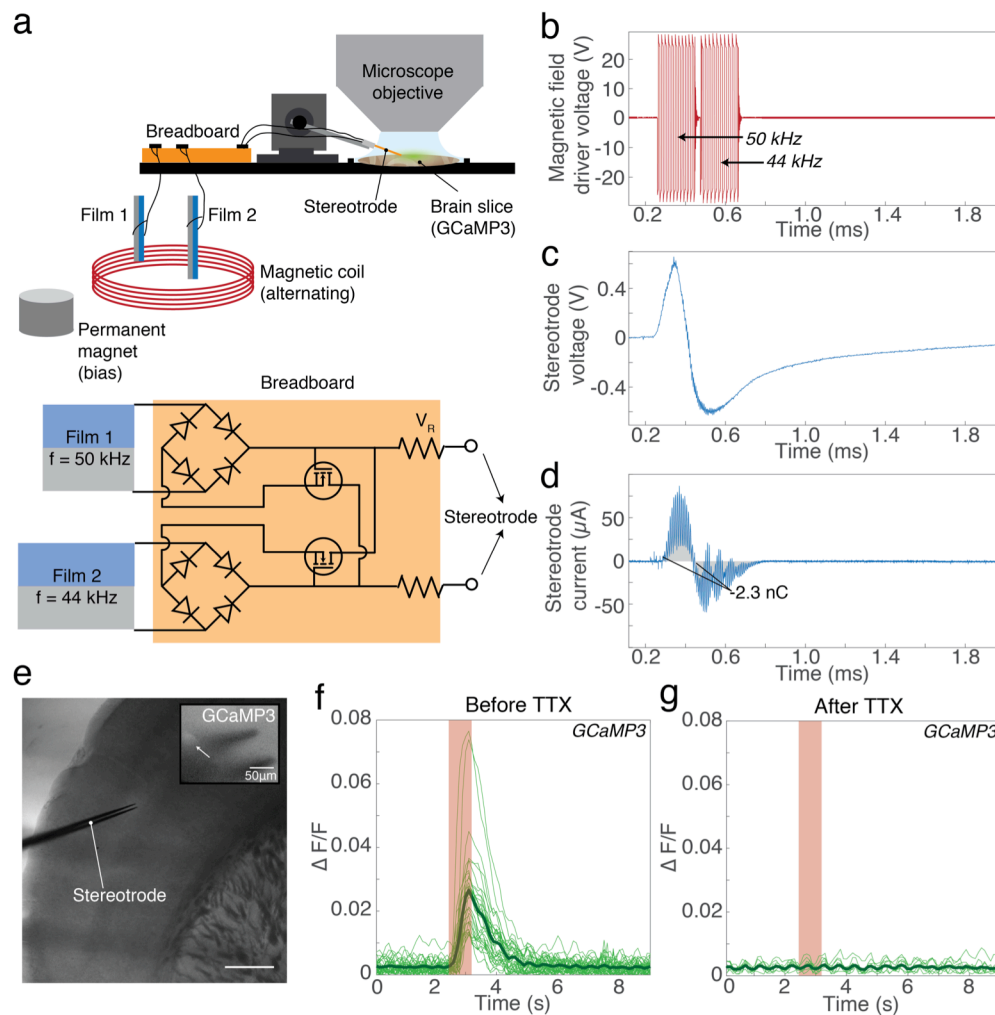307   nearby neurons.
308

Figure 3 | Biphasic ME stimulators activate neurons in ex vivo brain slices (a) Schematic of experimental setup with two ME films for biphasic stimulation (b) Measured voltage waveform produced by our magnetic field generator. When coupled to the magnetic coils, this waveform produces magnetic fields that alternate between the resonant frequencies of the two ME films (c) Measured voltage across the stereotrode shows the expected biphasic pulse shape (d) Calculated current based on measuring the voltage across our load resistor (V_R) shows nearly perfect charge balancing with only 2.3 nC accumulating on the electrode per pulse train. (e) Bright field image of stereotrode in mouse cortex (scale bar = 1 mm) with inset of GCaMP signal averaged over a 600 μm x 600 μm region around stereotrode tip. Arrow indicating a fluorescing cell body near the stereotrode (f) Average GCaMP signal when resonant magnetic field is applied before (f) and after (g) adding TTX shows neural activity is induced by the ME stimulator. Thin green traces represent separate experiments from two different brain slices, and thick black traces represent the mean of all experiments.

309
310

ME Neural Stimulation in Freely Moving Rats Shows Behavioral Efficacy

A major advantage of our ME stimulators is the fact that remote activation enables experiments with freely behaving animals. As a proof-of-principle we adapted our biphasic stimulator for deep brain stimulation (DBS) in freely moving rats (Fig. 4). To test ME stimulator efficacy, we used a previously reported protocol to test DBS in hemi-parkinsonian rats[36]. In these experiments rats are injected with 6-OHDA in the left medial forebrain bundle (MFB) to create a unilateral lesion of the substantia nigra pars compacta (SNc). The animals are then placed in a 30 cm diameter circular enclosure. Following a dose of methamphetamine, the hemi-parkinsonian rats have been shown to rotate ipsilateral to the injection (e.g. left for injection into the left MFB). During these rotations, the rat primarily moves using its contralateral (right) forepaw, rarely placing the ipsilateral (left) forepaw onto the ground. When a biphasic stimulus is applied at 200 Hz in the sub-thalamic nucleus (STN) using a tethered electrode array stimulator, rats typically stop turning to the left and exhibit more normal behavior such as moving with both forepaws, maintaining a steady orientation, or turning to the contralateral side[34].

To create a wireless, biphasic ME stimulator for freely moving animals we added a small permanent magnet to the ME stimulator to generate a bias field, and wrapped the behavioral chamber with 18 AWG copper wire to create a solenoid (Fig. 4a, S5). By integrating the small permanent magnet (< 0.25g) into the ME stimulator, we could ensure that the bias field was constantly aligned with ME films as the animal moved within the enclosure. We could also ensure that the positive and negative stimuli had equal amplitudes by independently adjusting the distance between each film and the permanent magnet. This ME stimulator was then connected to a commercial electrode array (Microprobes) implanted in the STN (Fig 4b, see Methods). We ensured that the stimulation voltage and current were within the safe and therapeutic range by measuring the output of the ME stimulator connected to an equivalent circuit model of the brain (Fig. 4c, see methods). Specifically, we observed peak voltages of approximately +/-1.5 V and peak currents of approximately +/- 100 µA for 400 us at approximately a 50% duty cycle (200 µs of overall current per phase), which is within the effective stimulation range reported for conventional wired stimulators[36]. When we tune the magnetic field frequency off resonance we observe almost no generated voltage or current (Fig. 4c).
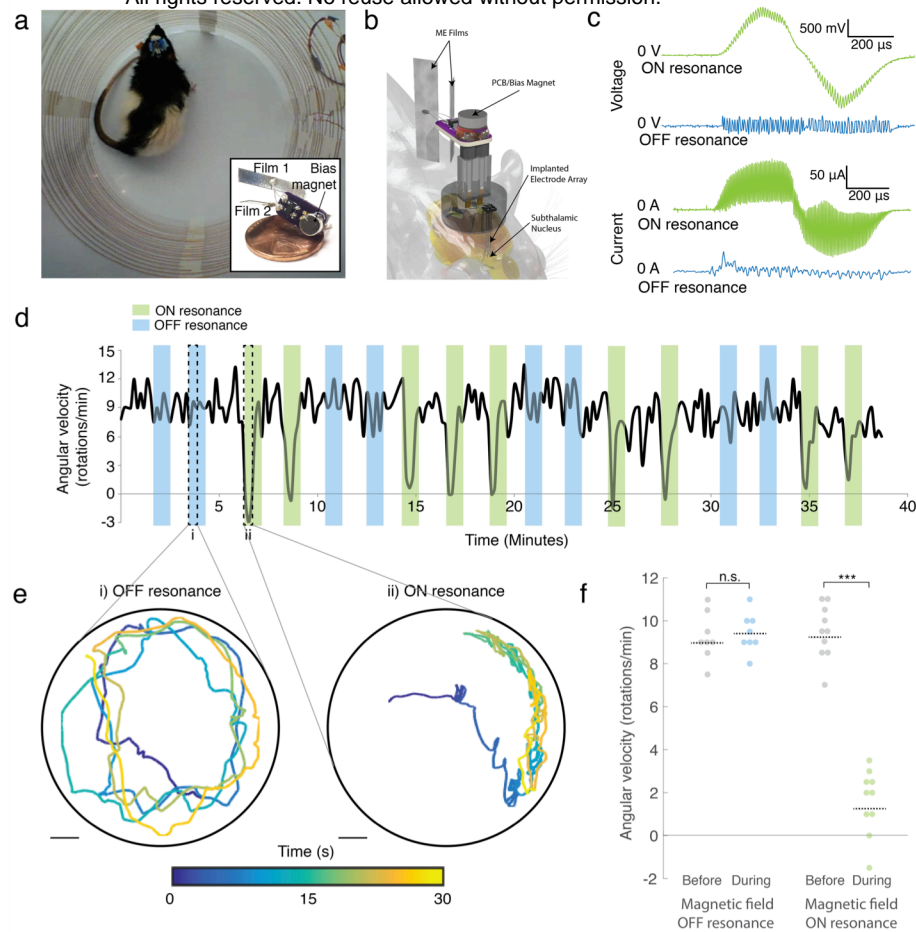
Figure 4 | Effective DBS in a freely moving rat using a wireless ME stimulator (a) Experimental setup showing rat in a circular enclosure wrapped with magnet wire. Inset shows a biphasic ME stimulator on a one cent coin (b) Schematic of the biphasic ME stimulator attached to the electrode array that is implanted into the STN (c) Measured voltage generated by the ME device and the current applied to the brain on resonance (green) and off resonance (blue). Approximately 100 µA biphasic stimulation is applied only when then the magnetic field frequency matches the resonance condition. (d) Angular velocity of the hemi-Parkinsonian rat over a 40 minute DBS trial with intervals of resonant and non-resonant stimulation shows that rotations are reduced only when the stimulator is activated by a resonant magnetic field (e) Typical trajectories show the location of the animal's head over two 30-second intervals denoted in c (scale bar = 5cm) (f) Average angular velocity of the rat during the 30 seconds before stimulation and the first 30 seconds of stimulation for each interval during the 40-min experiment shows a clear reduction in angular velocity only when the ME film is activated on resonance (*** P = 4x10^{-7}, n.s.=not significant P=0.70, paired t-test)

346
347 We then tested the wireless version of our biphasic ME stimulator mounted to the
348 head of a freely behaving rat and found that ME stimulation showed efficacy
349 comparable to previously reported wired DBS stimulators (Fig. 4). With a magnetic
350 field applied at resonance, we found that one-minute periods of 200 Hz biphasic
351 pulses resulted in a significant decrease in the animal's rotation rate (Fig. 4d green
352 intervals). This decreased rotation was not observed when the magnetic stimulus
353 frequency was tuned off resonance (Fig. 4d blue intervals). Plots of the head

354   trajectories show that the pathological rotations observed during off-resonant
355   magnetic field stimulation are not present when the ME stimulator is active during
356   resonant magnetic field stimulation (Fig. 4e, Methods). When averaged over all
357   trials, average rotation rate during the first half of stimulation fell to a statistically
358   significant 1.6 rotations per minute (rpm), compared to 9.3 rpm in the absence of
359   stimulation, or 9.4 rpm during off-resonant stimulation (paired t-test, Fig. 4f). We
360   further demonstrated the repeatability of this stimulator by repeating this
361   stimulation protocol on a second rat and found similar results (Fig S5b).
362
363   With a weight of 0.67 g, the ME stimulators described here are the first reported
364   miniature, magnetic, high frequency stimulator. Furthermore, by changing the
365   frequency and timing of the external drive coils, we can generate a variety of
366   stimulation patterns throughout the therapeutic window of 100-200 Hz with
367   applications to other disease models. Additionally, calculations of the magnetic field
368   strengths suggest that we can reconfigure the drive coils for a number of behavioral
369   experiments by placing coils beneath the floor of an animal enclosure. Finite
370   element simulations and measurements show that even at distance 4-5 cm above a
371   drive coil, ME films generate sufficient voltage for stimulation (Fig. S6). This
372   distance could be further improved by optimizing the geometry of the coils or
373   increasing the power of the magnetic field.
374
375   **Demonstration of multichannel deep brain stimulation in skull phantom using**
376   **rice-sized ME films**
377
378   In addition to supporting experiments in freely moving rodents, ME materials could
379   enable miniaturized wireless stimulators that operate deep in the brain of large
380   animals or human patients and are individually activated with an external
381   electromagnet. To our knowledge, this is the first technology that enables
382   independent external wireless control of multiple miniature stimulators deep
383   beneath a human skull phantom. Figure 5a shows the predicted depth that various
384   miniature antennas could be safely implanted under the skull and generate 1 mW of
385   power, which is in the approximate maximum power required for high-frequency
386   continuous neural stimulation[31]. As mentioned above, radio-frequency (RF)
387   powered antennas that operate at frequencies above ~1 MHz have limitations in the
388   amount of power that can safely be delivered to an implanted device without
389   causing potentially harmful tissue heating. Simulations show that when operating
390   with the safe power limits, RF-antennas must be placed on the surface of the brain
391   or in very shallow regions to harvest 1 mW of power. "Mid-field" techniques[37],
392   improve the RF coupling efficiency enabling deep operation, but because this
393   approach operates at a fixed frequency there have yet to be demonstrations of
394   individually addressable motes or biphasic stimulation. Other techniques for
395   wireless power delivery discussed previously, such magnetic induction, also cannot
396   achieve deep multichannel stimulation. For example, even using a higher operating
397   frequency of 1 MHz an inductive coil with the same orientation and cross-sectional
398   area as the ME films shown here would require a minimum of 500 turns of wire to
399   generate 2 V using the same 0.5 mT field used here (assuming a typical Q-factor of
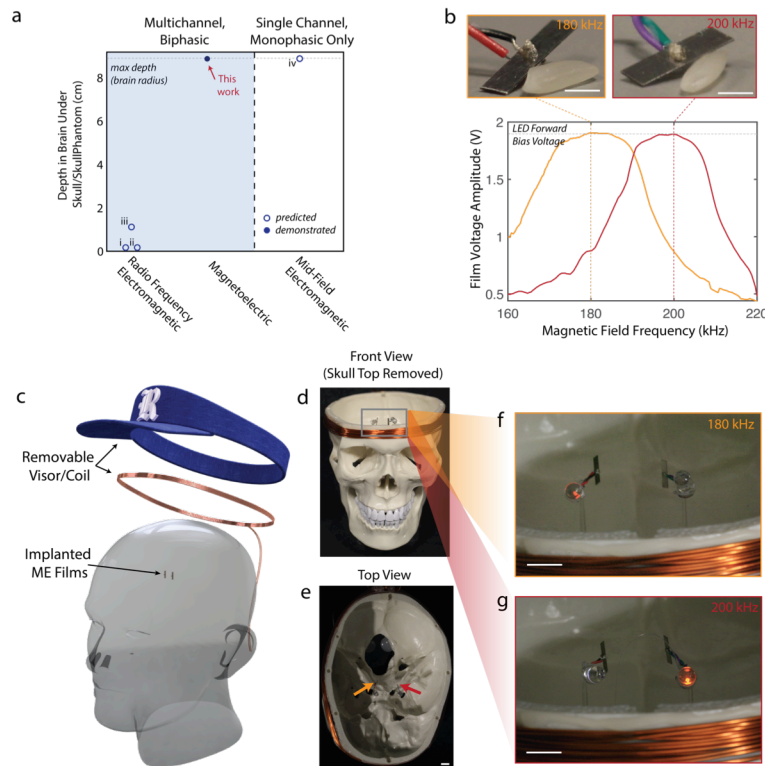
Figure 5 | Miniaturized Multichannel Stimulation in Human Skull Phantom (a) Comparison of effective depth beneath a human skull phantom for ME devices compared to other miniature wireless stimulators. Depth limit is based on safety limits to generate 1 mW. (i: Park et. al, *Proc Nat Ac Sci*, 2016 , ii:Yazdandoost et. al, *Asia Pac Microw Conf*, 2009, iii: Yazdandoost et. al, *Proc 37 Europ Microw Conf*, 2007, iv: Agrawal et. al, *Nat Biomed Eng*, 2017) (b) Photos of ME films next to a grain of rice and the corresponding voltage as a function of magnetic field frequency (field strength 1 mT, scale bars 2 mm) (c) Schematic of showing potential application of fully implanted ME films with the magnetic field generated by an external coil that can be incorporated into a hat or visor (d) Front view and (e) top view of skull phantom with the top removed to view LEDs (film locations indicated by arrows, scale bar 1 cm) (f) Photo of LEDs attached to ME films with the magnetic fields at applied at180 kHz and (g) 200 kHz. Selective illumination of the LEDs corresponding the resonant frequencies of the films demonstrates successful multichannel activation of individual films (scale bars 1 cm). Magnetic field strength was measured to be 0.5 mT at the location of the ME films.

400   10). Thus, devices based on magnetic inductors cannot be miniaturized without
401   sacrificing available power as described previously[9].
402
403   As a proof-of-concept demonstration we show that two rice-sized ME films can be
404   individually addressed at the center of a human skull phantom using an external
405   electromagnet. These two-films with lengths of 8 mm and 10 mm have acoustic
406   resonant frequencies of 180 and 200 kHz, which are determined by the film length.
407   When these films are attached to an orange LED, their output voltage is capped at
408   approximately 1.8 V, which helps to regulate the stimulation voltage and allows us
409   to visualize film activation. ME films of this size are smaller than current DBS leads
410   and could potentially be implanted into deep brain areas as shown in Fig 5c.
411   Additionally, the magnetic stimulation coil is small enough to be incorporated into a
412   stylish hat or visor that could be worn comfortably by a patient. When we placed

413   the two ME films at the center of a skull phantom we found that we could
414   individually illuminate the LEDs on each film when we applied a magnetic field at
415   the resonant frequency of the selected film (Fig 5d-g). For this experiment we used a
416   400 W power supply, which produced a field of approximately 0.5 mT at the center
417   of the skull phantom. The top of the skull phantom was removed for visualization,
418   but had no affect on our ability to drive the LED indicators. The number of
419   stimulation channels could be increased with the addition of ME films with different
420   resonant frequencies.
421
422   **Outlook**
423
424   To our knowledge, this is the first demonstration of a miniature, magnetic neural
425   stimulator that 1) operates in the therapeutic band (100-200 Hz) in freely moving
426   animals and 2) enables individually addressable miniature stimulators deep within
427   a human skull phantom; however, the advantages of ME materials extend beyond
428   these proof-of-principle demonstrations.
429
430   ME stimulators such as the one described in the in vivo rat experiment could have
431   an immediate impact on the study of DBS therapies using rodent disease models.
432   Because the ME stimulator is compatible with commercial implanted electrodes, and
433   the magnetic stimulators can be adapted to a number of standard behavioral
434   experiments or animal enclosures, our ME stimulators could readily replace the
435   wired DBS stimulators currently in use. As a result, new experiments can be
436   developed to probe the effects of chronic and continuous DBS or DBS in social
437   contexts where wired DBS stimulators would be impracticable.
438
439   Additionally, ME materials have the potential to enable miniature neural stimulators
440   that can be implanted deep in the brain of large animals or humans and addressed
441   externally with a small electromagnet. As shown here, rice-sized films can be
442   selectively activated based on unique resonant frequencies. Additional
443   miniaturization is not expected to reduce the voltage produced by these films since
444   the voltage depends on the thickness of the piezoelectric field and not the film
445   length (Fig. S2 c), suggesting that even smaller films could serve as effective
446   stimulators.
447
448   We also foresee applications for ME materials as a wireless power technology for
449   more complex implantable bioelectronic devices. For example, the demonstrated
450   ability of ME films to power LEDs implies that ME materials could power
451   implantable optogenetic stimulators, or small integrated circuits for physiological
452   monitoring.
453
454   To realize these fully implantable bioelectronic devices, work is needed to improve
455   ME materials and fabrication processes to reliably produce high-quality miniature
456   ME films, and encapsulate them for chronic use. For wearable technologies, it is also
457   necessary to further miniaturize magnetic field generators so that they can be

458 battery powered and comfortably worn. These advances must also be accompanied
459 by in vivo testing to show safety and efficiency for chronic use.
460
461 Overall, ME materials have the potential to fill a key need for wireless power
462 delivery to miniature biphasic neural stimulators and other bioelectronic devices
463 where the major challenge is transferring energy over distances of several
464 centimeters without heating the tissue or suffering loss at interfaces between tissue,
465 bone, and air.
466

467 **References**

468 1.   Hargreaves, D. G., Drew, S. J. & Eckersley, R. Kirschner Wire Pin Tract Infection
469   Rates: A randomized controlled trial between percutaneous and buried wires.
470   *J. Hand Surg. Br. Eur. Vol.* **29,** 374–376 (2004).

471 2.   Roy, B., C., M. D. & A., T. P. The brain tissue response to implanted silicon
472   microelectrode arrays is increased when the device is tethered to the skull. *J.*
473   *Biomed. Mater. Res. Part A* **82A,** 169–178 (2007).

474 3.   Markwardt, N. T., Stokol, J. & Rennaker, R. L. Sub-meninges implantation
475   reduces immune response to neural implants. *J. Neurosci. Methods* **214,** 119–
476   125 (2013).

477 4.   Sahin, M. & Pikov, V. Wireless Microstimulators for Neural Prosthetics. *Crit.*
478   *Rev. Biomed. Eng.* **39,** 63–77 (2011).

479 5.   Pinnell, R. C., Vasconcelos, A. P. De & Cassel, J. C. A Miniaturized ,
480   Programmable Deep-Brain Stimulator for Group-Housing and Water Maze
481   Use. *Front. Neurosci.* **12,** 1–11 (2018).

482 6.   Nurmikko, A. V. Approaches to large scale neural recording by chronic
483   implants for mobile BCIs. in *2018 6th International Conference on Brain-*
484   *Computer Interface (BCI)* 1–2 (2018). doi:10.1109/IWW-BCI.2018.8311503

485 7.   International, I. & Safety, E. *IEEE Standard for Safety Levels with Respect to*
486   *Human Exposure to Radio Frequency Electromagnetic Fields , 3 kHz to 300 GHz.*
487   **2005,** (2006).

488 8.   Fotopoulou, K. & Flynn, B. W. Wireless Power Transfer in Loosely Coupled
489   Links : Coil Misalignment Model. *IEEE Trans. Magn.* **47,** 416–430 (2011).

490 9.   Freeman, D. K. *et al.* A sub-millimeter, inductively powered neural stimulator.
491   *Front. Neurosci.* **11,** 1–12 (2017).

492 10.   De Hemptinne, C. *et al.* Therapeutic deep brain stimulation reduces cortical

493   phase-amplitude coupling in Parkinson's disease. *Nat. Neurosci.* **18,** 779–786
494   (2015).

495   11. Alonso, P. *et al.* Deep brain stimulation for obsessive-compulsive disorder: A
496   meta-analysis of treatment outcome and predictors of response. *PLoS One* **10,**
497   1–16 (2015).

498   12. Theodore, W. H. & Fisher, R. S. Review Brain stimulation for epilepsy. *Lancet*
499   **3,** 111–118 (2004).

500   13. Merrill, D. R., Bikson, M. & Jefferys, J. G. R. Electrical stimulation of excitable
501   tissue: Design of efficacious and safe protocols. *J. Neurosci. Methods* **141,** 171–
502   198 (2005).

503   14. Parastarfeizabadi, M. & Kouzani, A. Z. Advances in closed-loop deep brain
504   stimulation devices. *J. Neuroeng. Rehabil.* **14,** 79 (2017).

505   15. Montgomery, K. L. *et al.* Wirelessly powered, fully internal optogenetics for
506   brain, spinal and peripheral circuits in mice. *Nat. Methods* **12,** 969–974
507   (2015).

508   16. Ho, J. S. *et al.* Self-Tracking Energy Transfer for Neural Stimulation in
509   Untethered Mice. *Phys. Rev. Appl.* **24001,** 1–6 (2015).

510   17. Carrey, J. *et al.* Simple models for dynamic hysteresis loop calculations of
511   magnetic single-domain Simple models for dynamic hysteresis loop
512   calculations of magnetic single-domain nanoparticles : Application to
513   magnetic hyperthermia optimization. *J. Appl. Phys.* **83921,** (2015).

514   18. Chen, R., Romero, G., Christiansen, M. G., Mohr, A. & Anikeeva, P. Wireless
515   magnetothermal deep brain stimulation. *Science* **347,** 1477–80 (2015).

516   19. Munshi, R. *et al.* Magnetothermal genetic deep brain stimulation of motor
517   behaviors in awake, freely moving mice. *Elife* **6,** 1–26 (2017).

518   20. Johnson, B. C. *et al.* StimDust : A 6.5mm[3] , Wireless Ultrasonic Peripheral
519   Nerve Stimulator with 82 % Peak Chip Efficiency. *2018 IEEE Cust. Integr.*
520   *Circuits Conf.* (2018).

521   21. Seo, D. *et al.* Wireless Recording in the Peripheral Nervous System with
522   Ultrasonic Neural Dust. *Neuron* **91,** 529–539 (2016).

523   22. Piech, D. K. *et al.* StimDust: A 2.2 mm3, precision wireless neural stimulator
524   with ultrasonic power and communication. 1–35

525   23. Nan, T. *et al.* Acoustically actuated ultra-compact NEMS magnetoelectric

526   antennas. *Nat. Commun.* **8,** 1–7 (2017).

527   24.   O'Handley, R. C., Huang, J. K., Bono, D. C. & Simon, J. Improved Wireless,
528   Transcutaneous Power Transmission for *In Vivo* Applications. *IEEE Sens. J.* **8,**
529   57–62 (2008).

530   25.   Yue, K. *et al.* Magneto-Electric Nano-Particles for Non-Invasive Brain
531   Stimulation. *PLoS One* **7,** 1–5 (2012).

532   26.   Guduru, R. *et al.* Magnetoelectric 'spin' on stimulating the brain. *Nanomedicine*
533   **10,** 2051–2061 (2015).

534   27.   Ribeiro, C., Correia, V., Martins, P., Gama, F. M. & Lanceros-Mendez, S. Proving
535   the suitability of magnetoelectric stimuli for tissue engineering applications.
536   *Colloids Surfaces B Biointerfaces* **140,** 430–436 (2016).

537   28.   Zhai, J., Dong, S., Xing, Z., Li, J. & Viehland, D. Giant magnetoelectric effect in
538   Metglas/polyvinylidene-fluoride laminates. *Appl. Phys. Lett.* **89,** 8–11 (2006).

539   29.   Kulkarni, a. *et al.* Giant magnetoelectric effect at low frequencies in polymer-
540   based thin film composites. *Appl. Phys. Lett.* **104,** 0–5 (2014).

541   30.   Wan, C. & Bowen, C. R. Multiscale-structuring of polyvinylidene fluoride for
542   energy harvesting: the impact of molecular-, micro- and macro-structure. *J.*
543   *Mater. Chem. A* **5,** 3091–3128 (2017).

544   31.   Amar, A. Ben, Kouki, A. B. & Cao, H. Power approaches for implantable medical
545   devices. *Sensors (Switzerland)* **15,** 28889–28914 (2015).

546   32.   Park, J. *et al.* Screening fluorescent voltage indicators with spontaneously
547   spiking HEK cells. *PLoS One* **8,** 1–10 (2013).

548   33.   Jin, L. *et al.* Single Action Potentials and Subthreshold Electrical Events
549   Imaged in Neurons with a Fluorescent Protein Voltage Probe. *Neuron* **75,**
550   779–785 (2012).

551   34.   So, R. Q., Mcconnell, G. C. & Grill, W. M. Frequency-dependent , transient
552   effects of subthalamic nucleus deep brain stimulation on methamphetamine-
553   induced circling and neuronal activity in the hemiparkinsonian rat. *Behav.*
554   *Brain Res.* **320,** 119–127 (2017).

555   35.   Sun, Y. *et al.* Wirelessly Powered Implantable Pacemaker with On - Chip
556   Antenna. *IEEE* 1242–1244 (2017).

557   36.   Summerson, S. R., Aazhang, B. & Kemere, C. T. Characterizing Motor and
558   Cognitive Effects Associated With Deep Brain Stimulation in the GPi of Hemi-

559   Parkinsonian Rats. *IEEE Trans. Neural Syst. Rehabil. Eng.* **22,** 1218–1227
560   (2014).

561 37. Agrawal, D. R. *et al.* Conformal phased surfaces for wireless powering of
562   bioelectronic microdevices. *Nat. Biomed. Eng.* **1,** 1–16 (2017).

563 38. Schabrun, S. M., Jones, E., Elgueta Cancino, E. L. & Hodges, P. W. Targeting
564   chronic recurrent low back pain from the top-down and the bottom-up: a
565   combined transcranial direct current stimulation and peripheral electrical
566   stimulation intervention. *Brain Stimul* **7,** 451–459 (2014).

567 39. Mulpuru, S., Madhavan, M., McLeod, C., Cha, Y.-M. & Friedman, P. Cardiac
568   Pacemakers : Function , Troubleshooting , and Management. *J. Am. Coll.*
569   *Cardiol.* **69,** (2017).

570 40. Kesar, T. M. *et al.* Novel Patterns of Functional Electrical Stimulation Have an
571   Immediate Effect on Dorsiflexor Muscle Function During Gait for People
572   Poststroke. *Phys. Ther.* **90,** 55–66 (2010).

573 41. Bewernick, B. H. *et al.* Nucleus Accumbens Deep Brain Stimulation Decreases
574   Ratings of Depression and Anxiety in Treatment-Resistant Depression. *Biol.*
575   *Psychiatry* **67,** 110–116 (2010).

576 42. Park, S. Il *et al.* Stretchable multichannel antennas in soft wireless
577   optoelectronic implants for optogenetics. *Proc. Natl. Acad. Sci.* **113,** E8169–
578   E8177 (2016).

579 43. Yazdandoost, K. Y. A 2.4 GHz antenna for medical implanted communications.
580   *APMC 2009 - Asia Pacific Microw. Conf. 2009* 1775–1778 (2009).
581   doi:10.1109/APMC.2009.5384240

582 44. Yazdandoost, K. Y. & Kohno, R. An antenna for medical implant
583   communications system. *Proc. 37th Eur. Microw. Conf. EUMC* 968–971 (2007).
584   doi:10.1109/EUMC.2007.4405356

585

586

587   **Methods**
588
589   General Statistical Methods
590   Error bars in Figure S2fgdenote +/- one standard deviation for n=~50 data points.
591   We furthermore performed a Tukey's Honest Significant Difference test on the data
592   in Figure S2g, which indicated that the voltage produced at each different PVDF
593   thickness is significantly different. Paired t-tests were used for the rotation tests in
594   figure 4e.
595
596   Film Fabrication
597   To fabricate ME films, we used Metglas SA1 alloy (Metglas Inc) for the
598   magnetostrictive layer and polyvinylidenefluoride "PVDF" (precision acoustics) for
599   the piezoelectric layer. The PVDF films used for these experiments were pre-
600   stretched and poled by the manufacturer. The two layers were bonded together
601   using an epoxy capable of transferring the mechanical stress between the two layers
602   (Hardman double bubble red epoxy). Prior to bonding the two layers together, we
603   sputtered a thin layer of platinum (<100 nm) as a top electrode on the PVDF. Both
604   the Metglas and PVDF were plasma cleaned using O_2 plasma for five minutes before
605   epoxying. After the epoxy set, the films were cut into the desired rectangular shape
606   using scissors, taking care to cut the long axis of the film along the stretching
607   direction of the PVDF. We then attached wires using conductive epoxy to either side
608   of the films in order to measure the electrical capabilities of the film. We found that
609   attaching wires in the center dramatically increased the resonant voltage. However
610   for convenience, the wires were attached near the ends of the films during the in
611   vitro experiments. In many cases we also attached additional electronic components
612   such as diodes or LEDs to the wires attached to the films as noted in the appropriate
613   sections in the main text. Finally the devices were coated in 5-10 μm of parylene-C
614   (Labcoater 2). Initially this coating was used to electrically insulate and protect the
615   devices during in vitro experiments, but we also found that the encapsulation
616   increases the resonant voltage, which could be due to increased mechanical
617   coupling from the encapsulation.
618
619   Bench Top Electrolysis Tests
620   The stimulator shown in Fig 4a was wired to a stereotrode immersed in saline
621   under a microscope in order to observe the formation of bubbles from electrolysis
622   at the tips. During monophasic stimulation we used only one resonant frequency
623   and during biphasic stimulation we used two frequencies as demonstrated above. In
624   each case the pulse time was a 400 μs/phase. We determined the limit of
625   stimulation time as when the first bubble began to appear at the tips of the electrode
626   and repeated each data point 4 times.
627
628   Magnetic Field Generation (Fig. S3)
629   Each magnetic field generator consists of two major components, 1) Magnetic coils
630   used for the alternating magnetic field (described in the main text and optimized for
631   each experiment) and 2) Electronic drivers to control voltage and timing of the
632   alternating current in the coils (the same for all experiments).

633
634   To maintain simplicity, efficiency, and low cost the coils were driven with full H-
635   Bridge style switching circuits. The drivers are designed to deliver high currents to
636   the drive coils in the form of bi-phasic pulse trains. This reduces the cost and
637   complexity of the driver itself, as well as the power supply and control circuitry
638   when compared to arbitrary function generators. The design also has potential for
639   improved operational efficiency through impedance matching with the drive coils.
640   Furthermore, it is also possible to regulate power delivered to the drive coils on the
641   fly by adjusting the duty cycle of the current pulses, allowing power being delivered
642   to the ME film to be easily controlled digitally while maintaining the resonant
643   carrier frequency. The output carrier and pulse frequencies of the magnetic field are
644   generated using a TeensyLC board and custom Arduino code to generate the specific
645   pulse timings to deliver controlled ME stimulation (Fig. S3c,d).
646
647   These coils and drivers can be combined in different ways to generate the
648   appropriate field for a given experiment. For example, the setup used to generate
649   the alternating field in the in vivo rotation experiments consisted of four sets of coils
650   each with five turns powered by one driver with all four drivers synced to the same
651   output signal. In this way we can generate sufficient power to generate a mT-scale
652   magnetic fields over the whole behavioral area (Fig. S5a).
653
654   <u>Cell Culture</u>
655   For experiments performed on coverslips, HEK cells expressing sodium channel
656     $Na_{1.3}$ and potassium channel $K_{2.1}$ were grown on 12 mm poly-l-lysine coated
657   coverslips to approximately 30% confluency. The cells were then transfected with
658   the genetically encoded voltage indicator ArcLight using Lipofectamine (Invitrogen)
659   following manufacturer's recommendations. Two to three days after transfection
660   the coverslips were inverted onto ME films for testing. Preparation of GFP controls
661   followed the same procedure with the exception of replacing the ArcLight vector
662   (AddGene) with a GFP expression vector (AddGene). For experiments performed
663   with cells grown on the films, HEK cells transfected with ArcLight were placed onto
664   parylene coated poly-l-lysine treated films. The films were placed in cellular media
665   overnight and tested the following day.
666
667   ArcLight and GFP were excited at 460 nm with an LED light source. Fluorescence
668   images were collected at 33 fps using a CCD camera. Images were analyzed using
669   Matlab to quantify fluorescence changes in individual cells. In vitro testing was
670   performed in extracellular buffer (ECB, in mM: NaCl 119, KCl 5, Hepes 10, $CaCl_2$ 2,
671     $MgCl_2$ 1; pH 7.2; 320mOsm)
672
673   Figure S4b was obtained by growing unmodified HEK cells on a film submerged in
674   cellular media for five days. The cells were then stained with Hoechst and Calcein-
675   AM to label the nucleus and membrane respectively in living cells. The cells were
676   then fixed and imaged using a confocal microscope.
677
678

679   Mouse Brain Slice Procedures
680   We used 40 day old GAD2-GCaMP3 mice, generated by crossing GAD2-Cre (JAX #
681   10802) with flox-GCaMP3 (JAX # 14538) animals. Preparation of brain slices
682   followed procedures described by Ting et al.[45] and was carried out in accordance
683   with National Institutes of Health guidelines and approved by the UTHealth animal
684   welfare committee. Mice were deeply anesthetized with Isoflurane and perfused
685   with ice cold NMDG-based solution consisting of (in mM): 92 NMDG, 2.5 KCl, 1.25
686   NaH_2PO_4, 10 $MgSO_4$, 0.5 $CaCl_2$, 30 $NaHCO_3$, 20 glucose, 20 HEPES, 2 thiouera, 5 Na-
687   Ascorbate, 3 Na-pyruvate, saturated with 95% O_2 and 5% CO_2., at a rate of ~6
688   ml/min. Coronal brain slices (300 μm) were cut using a vibratome (Leica VT1200S),
689   incubated for 15 min at 35 °C in NMDG solution, and then transferred to a chamber
690   held at room temperature containing (in mM): 92 NaCl, 2.5 KCl, 1.25 NaH_2PO_4, 2
691   $MgSO_4$, 2 $CaCl_2$, 30 $NaHCO_3$, 25 glucose, 20 HEPES, 2 thiouera, 5 Na-Ascorbate, 3 Na-
692   pyruvate, saturated with 95% O_2 and 5% CO_2. For experiments, slices were placed
693   into a recording chamber perfused with ACSF containing (in mM): 126 NaCl, 2.5 KCl,
694   1.25 NaH_2PO_4, 2 $MgCl_2$, 2 $CaCl_2$, 26 $NaHCO_3$, 10 glucose), held at 32-34 °C using an
695   inline heater. NBQX (10 μM) was included in the bath solution to block AMPA
696   receptor-mediated synaptic transmission. The stereotrode was placed in layer 5 of
697   somatosensory (barrel) cortex.
698
699   GCaMP3 was excited at 460 nm with an LED light source. Fluorescence images were
700   collected at 9.8 fps using a CCD camera attached to an Olympus BX51WI microscope.
701   Images were analyzed using Matlab to quantify fluorescence changes in 600 x 600
702   μm regions around the stereotrode tips.
703
704
705   Implant Design and Rat Surgical Procedures
706
707   Two male Long-Evans rats (n ≈ 1, 400 g) were anesthetized with isoflurane gas. Five
708   percent isoflurane was used to induce anesthesia and two percent was used to
709   maintain anesthetic depth. Buprenorphine (0.04 mg/kg) was administered 30
710   minutes prior to ear bars for analgesia. 5 - 7 skull screws were placed to anchor the
711   electrode array. Skull screws were bound to skull with Metabond dental acrylic. A
712   craniotomy was made to accommodate the micro electrode array and expose an
713   injection site for neurotoxin. A 30 gauge needle bent at the tip cut and pulled away
714   the dura mater covering of the brain. Desipramine (DMI) reconstituted in saline at a
715   concentration of 15 mg/mL was injected IP to protect noradrenergnic neurons. The
716   dose of DMI was approximately 15 mg/kg and injected approximately 30 minutes
717   prior to administration of neurotoxin. To induce a hemiparkinsonian lesion, 8 ug of
718   6-hydroxydopamine (OHDA) at 2 ug/uL in saline was injected at 0.2 uL/min into the
719   mid forebrain bundle (MFB -1.2 ML, -4 AP, and -8.1 DV). STN stimulation was
720   delivered via a 2x2 platinum iridium microelectrode array (Microprobes) with 600 x
721   600 μm spacing of 75 μm electrodes. Each electrode had a nominal 10 kOhm
722   impedance. The electrode array was lowered to -2.6 ML, -3.6 AP, and approximately
723   -8.2 DV from bregma. The array was fixed to the skull with dental acrylic. All

724 experiments were approved by the Institutional Animal Care and Use Committee of
725 Rice University.
726
727 Prior to stimulating each rat with the magnetoelectric stimulator, the stimulator
728 power was estimated via a benchtop approximation of the rodent electrode
729 impedance. Constant current stimulation of the rodent brain with an A-M Systems
730 4100 stimulator produced characteristic voltage waveforms that approximated a
731 simplified parallel RC circuit. A 56 kOhm resistor, and 440 pF capacitor in parallel
732 closely approximated the impedance characteristics of the rat brain across the
733 stimulating electrodes. Using this circuit model, we estimated the field strengths and
734 pulse durations necessary to produce the desired stimulation effects and confirm
735 that the stimulation was charge balanced prior to rodent experimentation.
736
737 Rotation Test Experiments
738 Prior to performing the rotation tests the rat was briefly anesthetized with 5%
739 isoflurane gas and injected intraperitoneally (IP) with methamphetamine (0.31 ml
740 1.25 mg/kg) and the wireless biphasic stimulator was plugged into the implanted
741 electrode array. After the anesthesia had worn off (about 5-10 min) the rat was
742 placed in the cylindrical behavioral chamber. The magnetic field was applied over
743 the whole behavioral area to the films on the device (Fig S5a).
744
745 The magnetic field was applied on resonance and off resonance for one minute at
746 various times during the 40-minute trial. The resonant frequencies were 73 kHz and
747 77 kHz and the off resonant frequencies were 63 kHz and 87 kHz.
748
749 Rodent Tracking
750 Head position on the rotation task was generated using a slightly modified version
751 of DeepLabCut[46] to track ears, snout, and implant. A dataset totaling 286 frames
752 from both the on and off resonance rotation tasks was hand labeled and trained for
753 approximately 140,000 iterations.
754
755 Skull Phantom Demonstration
756 At the magnetic field frequencies used for this experiment bone and tissue are
757 effectively transparent[47], so we selected a life sized skull with the size of an average
758 human adult head as a phantom (Orient Infinity Limited). It was wrapped with 18
759 AWG magnet wire as shown in Fig 5. The coil consisted of four coils in parallel each
760 wired to an individual magnetic field driver. All drivers were wired to the same
761 input frequency signal and powered from the same power supply. The films were
762 suspended at the center of the skull phantom. Orange LEDs (Chanzon) with a diode
763 antiparallel were attached to the films for wireless verification of the voltage
764 generated by the films. For visualization purposes the skull top was removed to
765 better photograph the LED.
766
767
768
769

References

45. Ting, J. T., Daigle, T. L., Chen, Q. & Feng, G. Acute brain slice methods for adult and aging animals: application of targeted patch clampanalysis and optogenetics. *Methods Mol. Biol.* **1183,** 221–242 (2014).

46. Mathis, A. *et al.* Markerless tracking of user-defined features with deep learning. *arXiv [cs.CV]* 1–14 (2018).

47. Bottomley, P. A. & Andrew, E. R. RF magnetic field penetration, phase shift and power dissipation in biological tissue: Implications for NMR imaging. *Phys. Med. Biol.* **23,** 630–643 (1978).
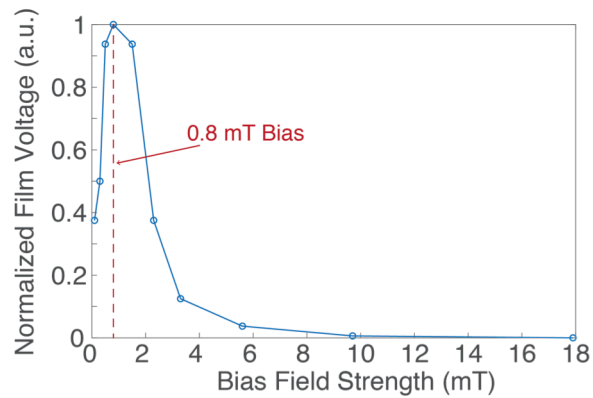
Supplemental Figure 1 | Film output voltage as a function of bias field The peak resonance voltage is significantly increased by a modest bias field that can be produced by a permanent magnet.
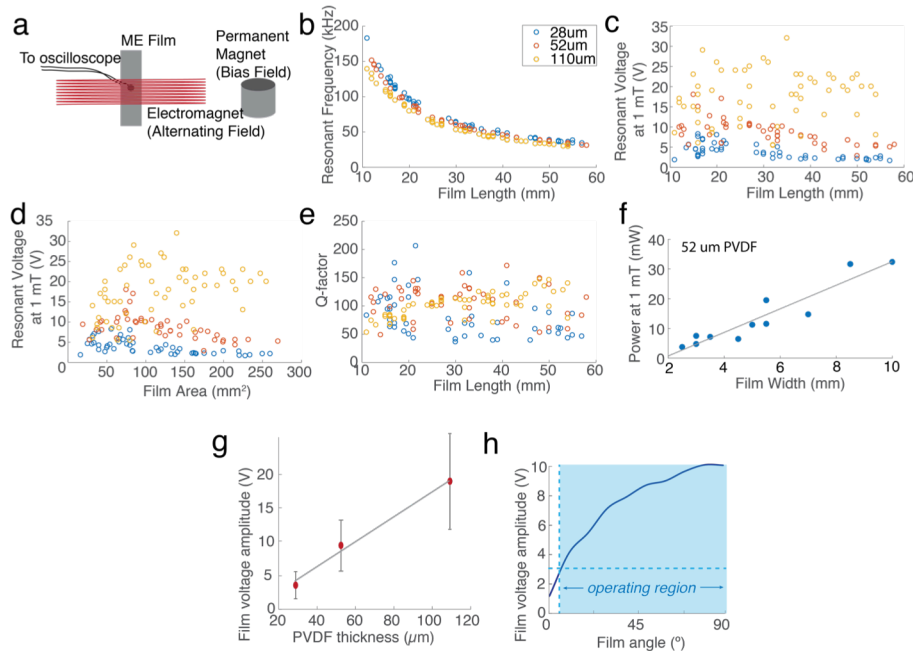

Supplemental Figure 2 | ME properties as a function of film size (a) Schematic of experimental setup used to gather data. Testing was performed for ME films with three different PVDF thicknesses: 28 (blue), 52 (red), and 110 (yellow) μ m (b) Resonant frequency as a function of film length (c) Output voltage as a function of film length (d) Output voltage as a function of film surface area (e) Q-factor as a function of film length (f) Maximum power output as a function of film width for 52um PVDF thickness (g) Peak resonant voltage plotted vs. PVDF thickness shows that the peak ME voltage increases with the PVDF thickness. Error bars indicate +/- 1 standard deviation for n ≈ 50 films for each thickness. (h)ME voltage as a function of angle between the film and the coil. Blue region shows the range of operating angles for which the voltage is greater than the expected stimulation voltage
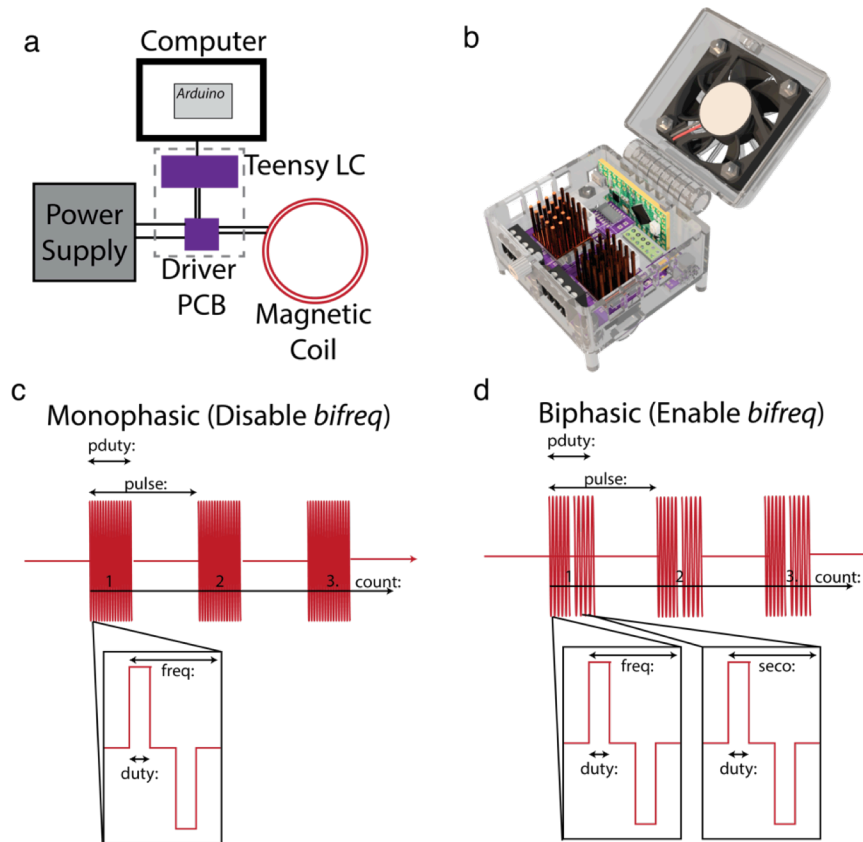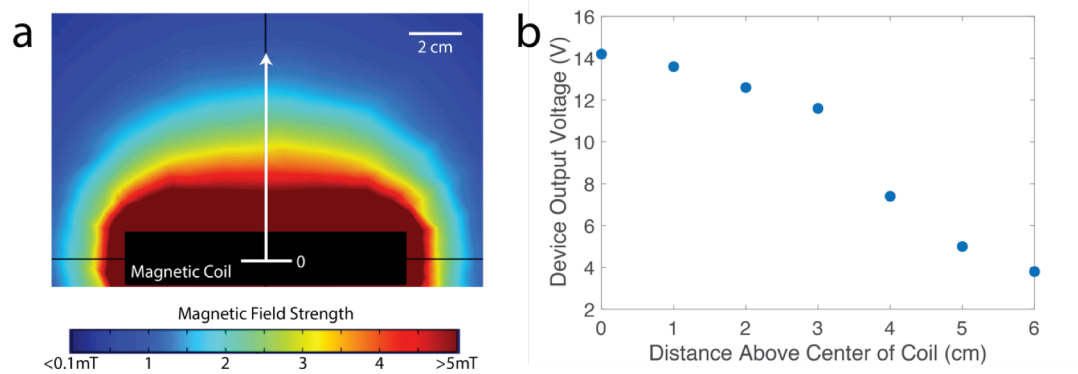
Supplemental Figure 3 | Magnetic Field Driver (a) Schematic of the major components of the magnetic field driver. Dashed line denotes components rendered in (b). (c) Output waveform for monophasic stimulation and the parameters that can be controlled by the drive software (d) Output waveform for biphasic stimulation, and the parameters that can be controlled by the driver software.
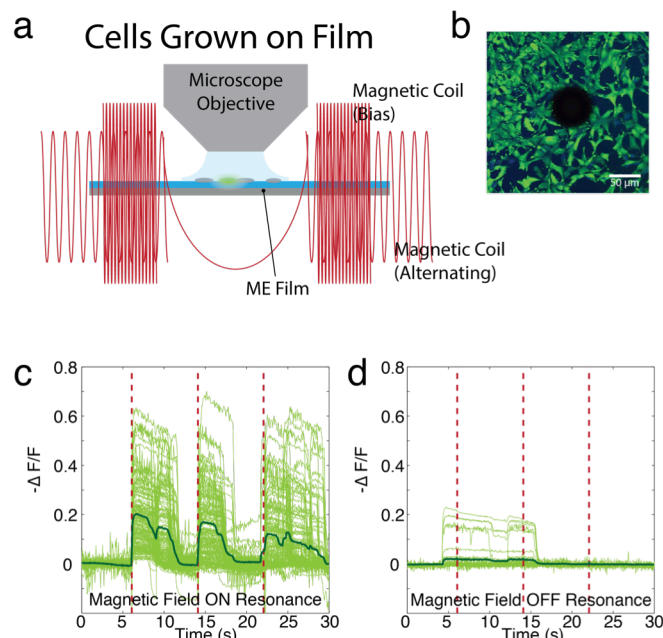
Supplemental Figure 4 | ME stimulation of cells grown directly on ME film (a) Schematic of experimental setup (b) Microscope image of fixed cells adherent to the region around a stamped hole (Hoechst/Calcein-AM, cells labeled prior to fixing) (c) ArcLight fluorescence of spiking HEK cells when magnetic field is on resonance and (d) off resonance.
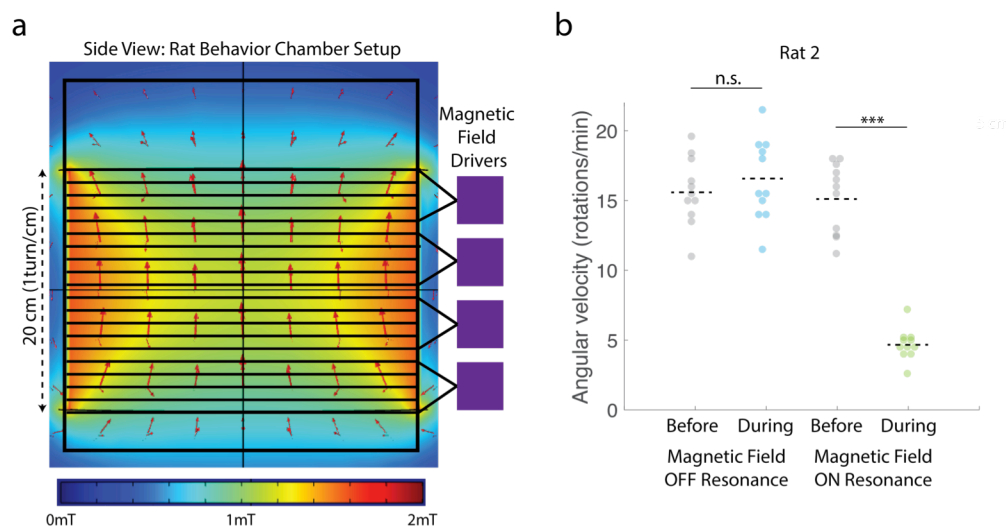
Supplemental Figure 5 | Magnetic Field for DBS Rotation Experiment (a) Schematic shows the location and spacing of wires and the number of drivers used to generate the alternating magnetic field overlaying a COMSOL simulation of magnetic field strength in the chamber (b) Results from rotation test in Rat 2: Angular velocity in the 30 seconds before stimulation and the first 30 seconds of stimulation shows a clear reduction in angular velocity only when the ME film is activated on resonance (*** P = 1.5x10^{-8}, n.s.=not significant P=0.27, paired t-test)

Supplemental Figure 6 | ME devices operate several centimeters above a single magnetic coil
(a) COMSOL simulation of magnetic field above a circular coil and (b) Measured device output voltage as a function of distance above the coil